







**Effect of curvature on the diffusion of colloidal bananas**Justin-Aurel Ulbrich <sup>1,2</sup>, Carla Fernández-Rico <sup>1,2,\*</sup>, Brian Rost,<sup>3</sup> Jacopo Vialetto <sup>2</sup>, Lucio Isa <sup>2</sup>,  
Jeffrey S. Urbach <sup>3,†</sup> and Roel P. A. Dullens <sup>1,4,‡</sup><sup>1</sup>*Department of Chemistry, Physical and Theoretical Laboratory, University of Oxford, South Parks Road, Oxford OX1 3QZ, United Kingdom*<sup>2</sup>*Department of Materials, ETH Zürich, 8093 Zurich, Switzerland*<sup>3</sup>*Department of Physics and Institute for Soft Matter Synthesis and Metrology, Georgetown University, Washington, DC 20057, USA*<sup>4</sup>*Institute for Molecules and Materials, Radboud University, Heyendaalseweg 135, 6525 AJ Nijmegen, The Netherlands*

(Received 8 November 2022; accepted 22 February 2023; published 21 April 2023)

Anisotropic colloidal particles exhibit complex dynamics which play a crucial role in their functionality, transport, and phase behavior. In this Letter, we investigate the two-dimensional diffusion of smoothly curved colloidal rods—also known as colloidal bananas—as a function of their opening angle  $\alpha$ . We measure the translational and rotational diffusion coefficients of the particles with opening angles ranging from  $0^\circ$  (straight rods) to nearly  $360^\circ$  (closed rings). In particular, we find that the anisotropic diffusion of the particles varies nonmonotonically with their opening angle and that the axis of fastest diffusion switches from the long to the short axis of the particles when  $\alpha > 180^\circ$ . We also find that the rotational diffusion coefficient of nearly closed rings is approximately an order of magnitude higher than that of straight rods of the same length. Finally, we show that the experimental results are consistent with slender body theory, indicating that the dynamical behavior of the particles arises primarily from their local drag anisotropy. These results highlight the impact of curvature on the Brownian motion of elongated colloidal particles, which must be taken into account when seeking to understand the behavior of curved colloidal particles.

DOI: [10.1103/PhysRevE.107.L042602](https://doi.org/10.1103/PhysRevE.107.L042602)

The Brownian motion of particles suspended in a fluid is a classic topic of study, describing the erratic, random motion of micron-sized particles colliding with the surrounding solvent molecules [1–3]. This type of motion has huge implications in the self-assembly, phase behavior, and transport properties of colloidal systems [4–7], and can be also used as a powerful tool to locally measure the rheology of complex fluids, such as the cell interior [8,9]. First discovered by Brown [10], and later formalized by Einstein [1], the extent of Brownian motion is described by the diffusion coefficient  $D$ , which for a sphere depends solely on the sphere's radius  $R$ , the temperature  $T$ , and viscoelasticity of the medium [11]. In the case of a Newtonian fluid, the diffusion coefficient of a sphere is related to the hydrodynamic drag  $\xi$  of the particle by famous the Stokes-Einstein relation  $D = k_B T \xi^{-1}$ , which can be experimentally measured from the mean-square displacement (MSD) of the particles in a solvent [1,4,7].

Introducing shape anisotropy in the particles has a dramatic impact on the way they diffuse. In fact, measuring the diffusion of nonspherical particles is an area of long-standing and ongoing research [12–25]. This is because many relevant microscopic building blocks, such as functional nanoparticles, protein fibrils, and colloidal molecules, are far from isotropic. The challenging step in this process is to determine the dif-

fusion coefficient of the particles along their different axes and measure the coupling between their translational and rotational motion [12,26]. To address this, laboratory and body frame coordinate systems are typically used to separately measure the MSDs along the directions corresponding to the particles' axes and decouple their rotational and translational motion [16,20,27]. For high-aspect-ratio uniaxial particles, such as colloidal ellipsoids and rods, the diffusion tensor is symmetric, meaning that there is no coupling between rotational and translational motion. In these systems, the diffusion along the long axis of the particles is higher than perpendicular to it [14–18,23]. For less symmetric shapes, such as biaxial particles, e.g., colloidal boomerangs [19–21], a similar trend is observed with higher diffusivity along the long axis. Nonetheless, the diffusion tensor is more complex and comprises off-diagonal elements accounting for translational-rotational coupling of the dynamics [19–21].

Recent advances in colloid synthesis have allowed to not only produce highly anisotropic particles with different symmetries [28,29], but also particles with a smooth and tunable curvature. This is the case of our recently developed system of *colloidal SU-8 bananas* [30], whose curvature is characterized by their opening angle  $\alpha$  [see Fig. 1(a)]. These polymer particles have already given valuable insight into the importance of  $\alpha$  in the structure of banana-shaped liquid crystals [30,31], but might also serve as model systems for other curved colloidal systems, such as bacteria [32,33] or curvature-mediating proteins [34,35]. This highlights the importance of uncovering their dynamical behavior as a function of their opening angle,

\*carla.fernandezrico@mat.ethz.ch

†urbachj@georgetown.edu

‡roel.dullens@ru.nl

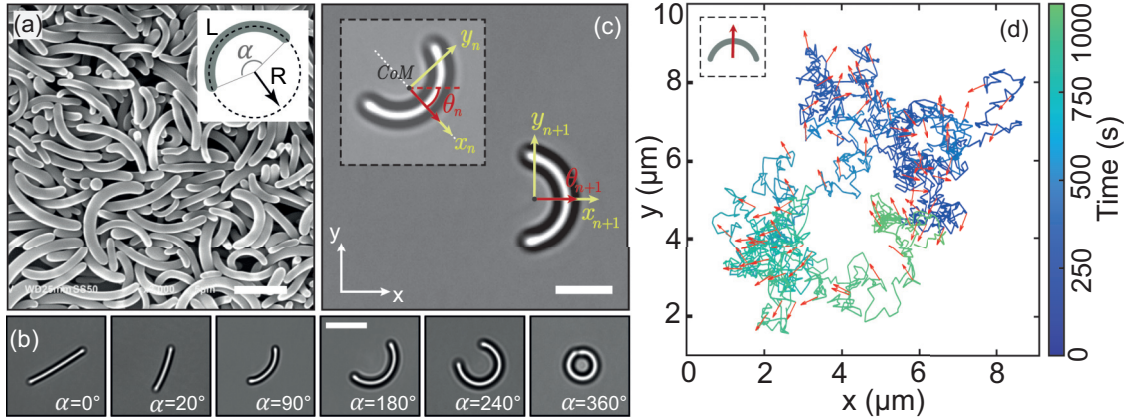


FIG. 1. Diffusion of colloidal SU-8 banana-shaped particles in two dimensions. (a) Typical scanning electron microscopy image of SU-8 colloidal bananas with an average length  $L$ , opening angle  $\alpha$ , and radius of curvature  $R$  (see inset). (b) Optical microscopy images of colloidal bananas with increasing opening angle  $\alpha$ . (c) Optical microscopy image of a colloidal banana undergoing Brownian motion in the  $xy$  plane in two different time points. The laboratory frame axes ( $x$  and  $y$ , white) are fixed, while the body frame axes ( $x_n$  and  $y_n$ , yellow) evolve with the particle's motion, where  $n$  is the frame number. We track the displacement of the center of mass (CoM) along  $x_{n+1}$  and  $y_{n+1}$ , and also their orientation  $\theta_n$ , defined as the angle between the  $x$  axis and the  $x_n$  axis. The red arrow and white dotted lines are the orientation vector of the particles and their symmetry axis, respectively. (d) Typical trajectory and orientation field of a diffusive colloidal banana over time. All scale bars are  $5 \mu\text{m}$ .

as previous studies have either focused on the role of the opening angle in short colloidal chains [24,25], whose geometry significantly differs from the smoothly curved bananas studied here, or on the dynamics of colloidal boomerangs with a single opening angle [19].

In this Letter, we investigate the two-dimensional diffusion of SU-8 colloidal bananas sedimented onto a solid surface, as a function of their opening angle  $\alpha$ . To this end, we use particles with  $\alpha$  ranging from  $0^\circ$  (straight rods) to nearly  $360^\circ$  (closed rings), and track their centers of mass in the  $xy$  plane over time using optical video microscopy (see Fig. 1). We find that the translational diffusion coefficient along the long axis of the particles,  $D_{yy}$ , is  $\sim 2.4$  times higher than that of the short axis,  $D_{xx}$ , for small  $\alpha$ , consistent with previous work on ellipsoids [17]. When  $\alpha$  increases, we observe that the ratio between the coefficients approaches unity, as also expected for closed ringlike objects. However, for  $\alpha > 180^\circ$ , we find a regime where the axis of fastest diffusion switches from the long to the short axis of the particles. In addition, we observe that the rotational diffusion coefficient  $D_\theta$  increases dramatically with increasing  $\alpha$ , and is about an order of magnitude larger for a nearly closed ring than for a rodlike particle of the same length. Finally, we find that our measurements are surprisingly well described by analytic results of the simplest form of slender body theory (SBT) [36–38], which allows us to conclude that the dynamical behavior of the particles primarily arises for the local drag anisotropy along the particles, with longer-range hydrodynamic couplings playing a secondary role.

A typical scanning electron microscopy image of the SU-8 colloidal bananas used for our diffusion experiments is shown in Fig. 1(a) (see synthesis details in Ref. [30]). The shape of the particles is described by a circular arc with a length  $L$ , opening angle  $\alpha$ , and radius of curvature  $R$  [see the inset of Fig. 1(a)]. Our colloidal bananas, which have an approximate diameter of  $1 \mu\text{m}$ , are polydisperse in size with lengths

ranging from  $8$  to  $12 \mu\text{m}$  ( $L/D \sim 10$ ) and opening angles ranging from  $0^\circ$  to  $360^\circ$  [see Fig. 1(b)]. We typically prepare very dilute particle suspensions in water (particle volume fraction  $\phi < 0.01$ ), and let the particles sediment towards the bottom surface of our sample cell. In order to confine the motion of the particles in two dimensions, we add a small amount of depletant ( $1 \text{ mg/mL}$  of aqueous xanthan solution) which introduces a weak depletion attraction ( $\sim 10k_B T$ ) between the particles and the cell wall [39], and suppresses any out-of-plane motion of the particles [40]. The resulting quasi-two-dimensional system is shown in Fig. 1(c), which shows an optical microscopy image of our system of colloidal bananas moving in the  $xy$  plane.

Next, we track the position and orientation of the particles over time, by measuring their center of mass (CoM) and orientation displacements using video optical microscopy [40,41] [see the resulting trajectory in Fig. 1(d)]. We extract the particles' translational and rotational diffusion coefficients by using particle tracking algorithms based on Chakrabarty's work [19,20]. The key parameters used for such measurements are shown in Fig. 1(c). In short, we use two coordinate systems, the laboratory frame, which is fixed over time [see white axes in Fig. 1(c)], and a continuous body frame, which is centered on the center of mass of the particle and moves with the particle's motion [see yellow axes in Fig. 1(c)]. Note that the body frame is always chosen such that its  $x$  axis  $x_n$  is parallel to the particle orientation vector [see the red arrow in Fig. 1(c)], which lies on the symmetry axis of colloidal bananas [see the dotted line in Fig. 1(c)].

The center-of-mass displacements in the body frame  $\delta \mathbf{r}(t)^{\text{BF}}$  are obtained using a rotational coordinate transformation of the displacements in the laboratory frame  $\delta \mathbf{r}(t)^{\text{LF}}$  following  $\delta \mathbf{r}(t)^{\text{BF}} = \mathbf{R}(\theta) \cdot \delta \mathbf{r}(t)^{\text{LF}}$ , where  $\delta \mathbf{r}(t) = (\delta x_n, \delta y_n)$  and  $\mathbf{R}(\theta)$  is the rotational transformation matrix [20]. Here,  $\theta$  is the particle orientation angle [see the angle in Fig. 1(c)], which is defined as the average angle between the final and

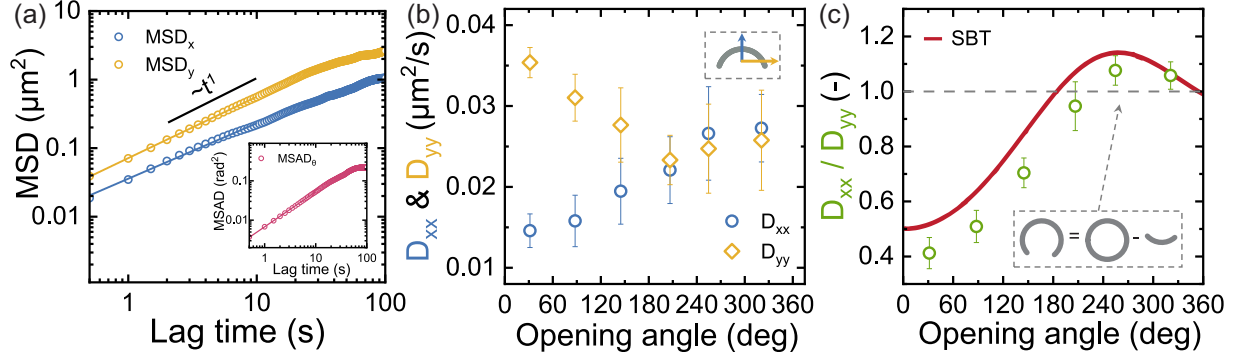


FIG. 2. Translational diffusion coefficients as a function of the opening angle  $\alpha$  of the particles. (a) Typical mean-squared displacement of a colloidal banana with  $\alpha = 100^\circ$  (note that the error bars are smaller than the symbols). The inset shows the angular MSD (MSAD). All curves show diffusive behavior ( $\propto t$ ) for lag times below 10 s. The lines show the best linear fit for short times where the fitting error is  $< 2\%$ . (b) Translation diffusion coefficients as a function of  $\alpha$ , along the short axis,  $D_{xx}$ , and the long axis,  $D_{yy}$ , of the particles. Each bin of  $60^\circ$  is averaged over  $\sim 15$  particles with a mean length of  $10 \pm 2 \mu\text{m}$ . The error bars represent the standard deviation. (c) Ratio of  $D_{xx}/D_{yy}$  as a function of  $\alpha$ . The solid line shows the analytical result from slender body theory (SBT) and the inset a sketch of a colloidal banana with a large opening angle.

initial orientations in the displacement of the particle. In this framework, the translation diffusion of the particle in the short axis,  $D_{xx}$ , is decoupled from the rotational diffusion  $D_\theta$  due to the symmetry of the particles [19,20]. On the contrary, the translational diffusion along the long axis,  $D_{yy}$ , remains coupled to the rotational diffusion regardless of the definition of  $\theta$ , unless the center of hydrodynamics (CoH) is used as the tracking point [19,20]. Nonetheless, as we discuss later in the text, this coupling is negligible as the distance between the CoM and CoH in our system is very small [see Fig. S2(a) [40]]. In the rest of this Letter, we use the methods explained above to systematically study how the translational and rotational diffusion coefficients are affected by the opening angle of the particles.

First, we consider the translational diffusion of the colloidal bananas. Figure 2(a) shows a representative mean-squared displacement (MSD) in the body reference frame of a colloidal banana with  $\alpha = 100^\circ$ . All MSD plots show diffusive behavior for lag times below 10 s. From short diffusion times [40], we extract the translational diffusion coefficients measured along the short,  $D_{xx}$ , and long axes of the particles,  $D_{yy}$ , as a function of the opening angle [see Fig. 2(b)]. First, we observe that  $D_{yy}$  largely exceeds  $D_{xx}$  for small opening angles. This behavior is expected, as for a rodlike particle ( $\alpha \sim 0^\circ$ ), the diffusion along the long axis is known to be approximately twice the diffusion along its short axis [15,17]. For large opening angles, the difference between  $D_{xx}$  and  $D_{yy}$  decreases, which is also expected as for a ring ( $\alpha \sim 360^\circ$ ),  $D_{xx} = D_{yy}$  due to symmetry reasons. Note that the scatter in the diffusion coefficient values, represented as the standard deviation in the error bars in Fig. 2(b), originates primarily from the polydispersity ( $\sim 20\%$ ) in the particles' length in each bin.

Interestingly, we find that for opening angles above  $200^\circ$ , the axis of fastest diffusion switches from the long to the short axis of the particles, with  $D_{xx}$  exceeding  $D_{yy}$  [see Fig. 2(b),  $\alpha > 200^\circ$ ]. This effect shows up more clearly in Fig. 2(c), where we plot the ratio of  $D_{xx}/D_{yy}$  as a function of the opening angle. First, we observe that the variance is substantially re-

duced as the ratio is insensitive to the length polydispersity of the particles, and secondly that this clearly exceeds unity for  $200^\circ < \alpha < 360^\circ$  with mean values of  $1.076 \pm 0.019$  ( $N = 10$ ) and  $1.057 \pm 0.018$  ( $N = 8$ ) for the largest two opening angles, where the uncertainty is the standard error. For  $\alpha \sim 360^\circ$ ,  $D_{xx}/D_{yy}$  approaches unity again, as expected for a ring. The nonmonotonical behavior of the measured anisotropic diffusion can be explained in terms of drag forces. For a ring, the drag force experienced by the particle is independent of the direction of motion, and therefore  $D_{xx} = D_{yy}$ . However, when a small segment of the ring is removed, the resulting translational diffusion of the broken ring becomes anisotropic with  $D_{xx} > D_{yy}$ . This is because the section removed has a lower longitudinal drag force than the transverse one ( $D_{yy} > D_{xx}$ ), and therefore the  $D_{xx}$  of the broken ring is reduced less than its  $D_{yy}$  [see a sketch of the broken ring in the inset of Fig. 2(c)].

This behavior is surprisingly well captured by the simplest form of slender body theory [see the solid line in Fig. 2(c)], which considers the hydrodynamic behavior of an infinitesimally thin banana, assuming that the perpendicular drag force of the body is twice the parallel one, and that there are no couplings between the different parts of the body [36–38,40]. The observed deviations from the experimental results stem from the fact that our particles are obviously not infinitesimally thin, from the presence of a depletant and from wall effects. In fact, our experimental results agree with previous experimental studies of confined ellipsoids [17,27], where an enhanced diffusion along the long axis is measured with  $D_{xx}/D_{yy} < 0.5$  due to the presence of a wall, a behavior that is not captured by the theoretical values shown here.

Next, we study the dependence of the rotational diffusion coefficient  $D_\theta$  on the opening angle of the particles. As shown in Fig. 3(a), we find that the rotational diffusivity of the colloidal bananas increases dramatically with increasing opening angle. In fact, this effect shows up more clearly when the expected length dependence is accounted for by multiplying  $D_\theta$  by  $L^3$ , where  $L$  is the arc length of each particle, and then normalizing it by the average  $D_\theta L^3$  measured for 20

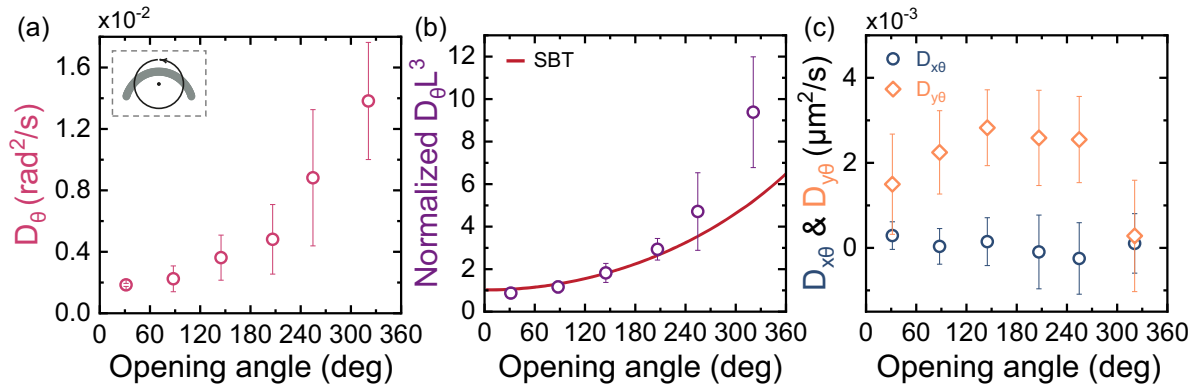


FIG. 3. (a) Rotational diffusion and coupling coefficients for colloidal bananas as a function of their opening angle. (a) Rotational diffusion  $D_\theta$  as a function of  $\alpha$ . Each bin of  $60^\circ$  is averaged over approximately 15 particles with a mean length of  $10 \pm 2 \mu\text{m}$ . (b)  $D_\theta$  times  $L^3$  for each particle, normalized by the average value of  $D_\theta L^3$  measured for rods ( $N = 20$ ). Solid line: Analytical result from slender body theory. (c) Translational-rotational coupling diffusion coefficients as a function of the opening angle. While no coupling is observed between rotations and the short axis of the particles, a nonzero coupling is observed for intermediate opening angles. The error bars represent the standard deviation of the average value.

straight rods [see Fig. 3(b)]. We find that  $D_\theta$  is about an order of magnitude larger for a ring than for a rod of the same length [ $D_\theta^{\text{ring}}/D_\theta^{\text{rod}} \approx 10$ , see Fig. 3(b)]. Part of this increase can be understood in the context of SBT [see the solid line in Fig. 3(b)], which not only considers drag forces but also torques introduced by small rotations of the particles around their center of mass [40]. When accounting for these two factors, SBT predicts that  $D_\theta^{\text{ring}}/D_\theta^{\text{rod}} \approx 6.6$ , for particles with the same length [40]. However, this result clearly underestimates our measurements for  $D_\theta$  at large opening angles [see Fig. 3(b),  $\alpha > 240^\circ$ ], which may be explained by the emergence of hydrodynamic coupling between the different parts of the particles as  $\alpha$  increases, or by an enhanced anisotropic diffusion near solid surfaces [17]. These effects may reduce the rotational drag of the particles and lead to the observed enhanced rotational diffusion for large opening angles.

Finally, we measure the coupling between the translational and rotational diffusion as a function of the opening angle, as shown in Fig. 3(c). Indeed, we find that such coupling is approximately zero between the short axis and the orientation of the particles,  $D_{x\theta}$ , for all opening angles [20]. We also find that there is a nonzero coupling between the long axis and rotation of the particles,  $D_{y\theta}$ , which is expected as we are using the center of mass and not the center of hydrodynamics as the tracking point [20]. Nonetheless, such coupling is nearly zero for small and large opening angles [see Fig. 3(c) for  $\alpha \sim 0^\circ$  and  $\alpha \sim 360^\circ$ ] and an order of magnitude smaller than  $D_{yy}/L$

for intermediate opening angles [see Fig. S2(b) [40]], which means that the trends described previously in Fig. 2 are indeed not significantly affected by this coupling.

In summary, we have measured the translational and rotational diffusion coefficients of smoothly curved colloidal bananas in two dimensions, as a function of their opening angle  $\alpha$ . We find that the typical anisotropic diffusion expected for straight rods decreases with increasing opening angle until  $\alpha > 180^\circ$ , at which point the axis of fastest diffusion switches from the long to the short axis of the particle. We also find that the rotational diffusion coefficient increases dramatically as the opening angle increases. We show that both observations are well described by the simplest form of slender body theory, indicating that these effects can be mainly understood by local drag forces along the particle. These results demonstrate key role of curvature on the Brownian motion of elongated particles, and highlights the richness in the diffusive behavior of colloids with curved shapes, including colloidal molecules, bacteria, or functional nanoparticles.

Laura Alvarez is thanked for useful discussions. R.P.A.D. and C.F.R. acknowledge the European Research Council (ERC Consolidator Grant No. 724834) for financial support. J.A.U. acknowledges financial support from the Fondation Zdenek et Michaela Bakala. B.R. and J.S.U. acknowledge support from the National Science Foundation (Grant No. ENG-1907705).

J.-A.U. and C.F.-R. contributed equally to this work.

- [1] A. Einstein, *Ann. Phys.* **322**, 549 (1905).
- [2] W. C. Poon, in *The Oxford Handbook of Soft Condensed Matter*, edited by E. M. Terentjev and D. A. Weitz (Oxford University Press, Oxford, UK, 2015), p. 1.
- [3] P. Hänggi and F. Marchesoni, *Chaos* **15**, 026101 (2005).
- [4] D. F. Evans and H. Wennerstrom, *The Colloidal Domain: Where Physics, Chemistry, Biology and Technology Meet* (Wiley-VCH, New York, 1999).
- [5] M. A. Boles, M. Engel, and D. V. Talapin, *Chem. Rev.* **116**, 11220 (2016).
- [6] V. N. Manoharan, *Science* **349**, 1253751 (2015).
- [7] W. Poon, *Science* **304**, 830 (2004).
- [8] D. Wirtz, *Annu. Rev. Biophys.* **38**, 301 (2009).
- [9] F. M. Hameed, M. Rao, and G. V. Shivashankar, *PLoS ONE* **7**, e45843 (2012).
- [10] R. Brown, *Philos. Mag.* **4**, 161 (1828).

- [11] T. G. Mason and D. A. Weitz, *Phys. Rev. Lett.* **74**, 1250 (1995).
- [12] H. Brenner, *J. Colloid Interface Sci.* **23**, 407 (1967).
- [13] W. A. Wegener, *Biopolymers* **20**, 303 (1981).
- [14] M. M. Tirado, C. L. Martínez, and J. G. de la Torre, *J. Chem. Phys.* **81**, 2047 (1984).
- [15] M. Doi and S. F. Edwards, *The Theory of Polymer Dynamics* (Clarendon Press, Oxford, UK, 1986).
- [16] Y. Han, A. M. Alsayed, M. Nobili, J. Zhang, T. C. Lubensky, and A. G. Yodh, *Science* **314**, 626 (2006).
- [17] Y. Han, A. Alsayed, M. Nobili, and A. G. Yodh, *Phys. Rev. E* **80**, 011403 (2009).
- [18] J. T. Padding and W. J. Briels, *J. Chem. Phys.* **132**, 054511 (2010).
- [19] A. Chakrabarty, A. Konya, F. Wang, J. V. Selinger, K. Sun, and Q. H. Wei, *Phys. Rev. Lett.* **111**, 160603 (2013).
- [20] A. Chakrabarty, A. Konya, F. Wang, J. V. Selinger, K. Sun, and Q. H. Wei, *Langmuir* **30**, 13844 (2014).
- [21] S. Delong, F. Balboa Usabiaga, and A. Donev, *J. Chem. Phys.* **143**, 144107 (2015).
- [22] Y. Yang and M. A. Bevan, *J. Chem. Phys.* **147**, 054902 (2017).
- [23] F. Roosen-Runge, P. Schurtenberger, and A. Stradner, *J. Phys.: Condens. Matter* **33**, 154002 (2021).
- [24] R. W. Verweij, P. G. Moerman, N. E. G. Ligthart, L. P. P. Huijnen, J. Groenewold, W. K. Kegel, A. van Blaaderen, and D. J. Kraft, *Phys. Rev. Res.* **2**, 033136 (2020).
- [25] R. W. Verweij, P. G. Moerman, L. P. P. Huijnen, N. E. G. Ligthart, I. Chakraborty, J. Groenewold, W. K. Kegel, A. van Blaaderen, and D. J. Kraft, *J. Phys. Mater.* **4**, 035002 (2021).
- [26] D. J. Kraft, R. Wittkowski, B. ten Hagen, K. V. Edmond, D. J. Pine, and H. Löwen, *Phys. Rev. E* **88**, 050301(R) (2013).
- [27] Z. Zheng and Y. Han, *J. Chem. Phys.* **133**, 124509 (2010).
- [28] T. Hueckel, G. M. Hocky, and S. Sacanna, *Nat. Rev. Mater* **6**, 1053 (2021).
- [29] S. C. Glotzer and M. J. Solomon, *Nat. Mater.* **6**, 557 (2007).
- [30] C. Fernandez-Rico, M. Chiappini, T. Yanagishima, H. de Sousa, D. G. L. Aarts, M. Dijkstra, and R. P. A. Dullens, *Science* **369**, 950 (2020).
- [31] C. Fernandez-Rico and R. P. A. Dullens, *Proc. Natl. Acad. Sci. USA* **118**, e2107241118 (2021).
- [32] A. Persat, H. A. Stone, and Z. Gitai, *Nat. Commun.* **5**, 3824 (2014).
- [33] R. Schuech, T. Hoehfurtner, D. J. Smith, and S. Humphries, *Proc. Natl. Acad. Sci. USA* **116**, 14440 (2019).
- [34] B. Qualmann, D. Koch, and M. M. Kessels, *EMBO J.* **30**, 3501 (2011).
- [35] Y.-B. Shen and Z. Shen, *Trends Cell Biol.* **25**, 59 (2015).
- [36] J. Gray and G. J. Hancock, *J. Exp. Biol.* **32**, 802 (1955).
- [37] B. Rodenborn, C.-H. Chen, H. L. Swinney, B. Liu, and H. P. Zhang, *Proc. Natl. Acad. Sci. USA* **110**, E338 (2013).
- [38] B. Rost, J. T. Stimatzke, D. A. Egolf, and J. S. Urbach, *Phys. Rev. E* **102**, 023103 (2020).
- [39] H. N. W. Lekkerkerker, W. C.-K. Poon, P. N. Pusey, A. Stroobants, and P. B. Warren, *Europhys. Lett.* **20**, 559 (1992).
- [40] See Supplemental Material at <http://link.aps.org/supplemental/10.1103/PhysRevE.107.L042602> for further details on the experiments, image analysis, and theory.
- [41] J. C. Crocker and D. G. Grier, *J. Colloid Interface Sci.* **179**, 298 (1996).